5 Noninvasive Imaging Techniques of Metal Nanoparticles and Their Future Diagnostic Applications

Sourav Das, Rajesh Kotcherlakota, and Chitta Ranjan Patra

Abbreviations

ABC	Accelerated blood clearance
AgNPs	Silver nanoparticles
AuNPs	Gold nanoparticles
CARS	Coherent anti-Stokes Raman scattering
CeO2	Cerium dioxide
CNS	Central nervous system
CT	Computed tomography
ESIONs	Extremely small iron oxide nanoparticles
FDA	Food and drug administration
FITC	Fluorescein isothiocyanate
FRET	Fluorescence resonance energy transfer
GBNs	Gadolinium based-nanoparticles
GSH	Glutathione
IgG	Immunoglobulin G
IGT	Image guided therapy
LLC	Lewis lung carcinoma
MAP	Maximum intensity projections
MCS	Merocyanines
MPR	Magnetic resonance-photoacoustic-Raman

S. Das · R. Kotcherlakota (✉) · C. R. Patra (✉)
Department of Applied Biology, CSIR-Indian Institute of Chemical Technology, Hyderabad, Telangana, India

Academy of Scientific and Innovative Research (AcSIR), Ghaziabad, UP, India
e-mail: crpatra@iict.res.in

A. K. Shukla (ed.), *Medical Imaging Methods*,
https://doi.org/10.1007/978-981-13-9121-7_5

MRgFUS	Magnetic resonance-guided focused ultrasound
MRI	Magnetic resonance imaging
MRS	Magnetic relaxation switch
MSOT	Multispectral optoacoustic tomography
NIH	NIH-3T3- Mouse embryonic fibroblast cell line
OCT	Optical coherence tomography
PAA	Polyacrylic acid
PAI	Photoacoustic imaging
PEG	Polyethylene glycol
PLGA	Poly(lactic-co-glycolic acid)
PSMA	Prostate-specific membrane antigen
QDs	Quantum dots
SCC	Squamous cell carcinoma
SERS	Surface-enhanced Raman spectroscopy
SiNPs	Silica nanoparticles
SKOV3	Human breast cancer cell line
SLN	Sentinel lymph node
SPIONs	Superparamagnetic iron oxide nanoparticles
SP-PCL	Spiropyran-terminated poly(ε-caprolactone)
$Ti(SP)_4$	Tetra spiropyran titanate
TiO2	Titanium oxide
UCL	Upconversion luminescence
UCNPs	Upconversion nanoparticles
ZnO	Zinc oxide

5.1 Background of Bio-imaging

Bio-imaging aids in diagnosis of diseases using less invasive methods and specific image guided treatments [1]. The fields of biology and medicine require bio-imaging to visualize the anatomical structures and their function for diagnosis of the disease and treatment. Medical imaging is an interdisciplinary field that employs the basis of physics, statistics, mathematics, computer science, radiology, biology, nuclear medicine, etc. [2]. Several technological advancements occurred over the last several decades and emerged with new applications [2]. Significant development has been shown in the field of bio-imaging over the last 50 years. The discovery of X-ray in 1895 by Wilhelm Conrad Roentgen has revolutionized the area of bio-imaging which further strengthened by contrast agents used to visualize bones and blood vessels [3]. Further, nuclear biomedical imaging method has emerged as potent technique with the use of gamma cameras. By 1906–1912, the application of pharmaceutical contrast agents advanced the field of medical radiography for imaging blood vessels and organs in the body. From 1971 to present, many other imaging techniques are implemented in medical imaging in order to improve the image quality and explore various advancements. Different bio-imaging techniques that are

being used are X-ray-based imaging, magnetic resonance imaging (MRI), fluorescence-based imaging, computed tomography (CT), Raman based imaging, luminescence upconversion imaging, etc.[4].The following section describes the applications of various bio-imaging methods.

5.1.1 Types of Bio-imaging

The techniques of various bio-imaging methods used for the diagnosis of the different diseases are described below:

- **Computed tomography (CT):** From the introduction in 1970s, CT has modernized the disease diagnosis [5]. CT has many applications than other imaging methods because of its lesser time to perform and mostly available to doctors for conforming the diseases [6].
- **X-ray microscopy:** This is an important tool for cellular imaging. X-rays generally obviate the need of sectioning of the specimens as they can penetrate easily into the thick biological samples [7].
- **Magnetic resonance imaging (MRI):** MRI employs a magnetic field and radio waves for imaging organs and tissues of the body. This imaging technique has changed the field of diagnosis by avoiding the exposure to harmful ionizing radiation [8].

Other techniques are demonstrated in the latter sections of this review article.

5.2 Nanotechnology and Its Role in Bio-imaging

Nanotechnology plays crucial role in bio-imaging. The following sections will discuss the various roles of nanoparticles in bio-imaging use in different techniques.

5.2.1 Metal-Based Nanoparticles for Bio-imaging

Over the past decades, the field of nanotechnology has been grown in a wide range for various fields. Multifunctional metal-based nanoparticles are introduced by various scientists all over the world to treat various diseases such as cancer, diabetes, cardiovascular diseases, etc. [9–11]. The diagnosis and the therapy as well as monitoring the therapeutic efficacy of various diseases became fruitful after the usage of various imaging techniques. The high surface to volume ratio, size, and solubility of nanoparticles help in moderating the pharmacodynamics and pharmacokinetics profiles of various agents (therapeutic, imaging) in enhancing their therapeutic efficacy [12]. Researchers are still probing new nanomaterials for better efficacy in therapeutic as well as diagnostic purpose. Figure 5.1 shows the usage of inorganic nanoparticles for therapy and imaging of tumor [12]. It has been observed that due to the tunable size, easy fabrication, generation of ROS (reactive oxygen species),

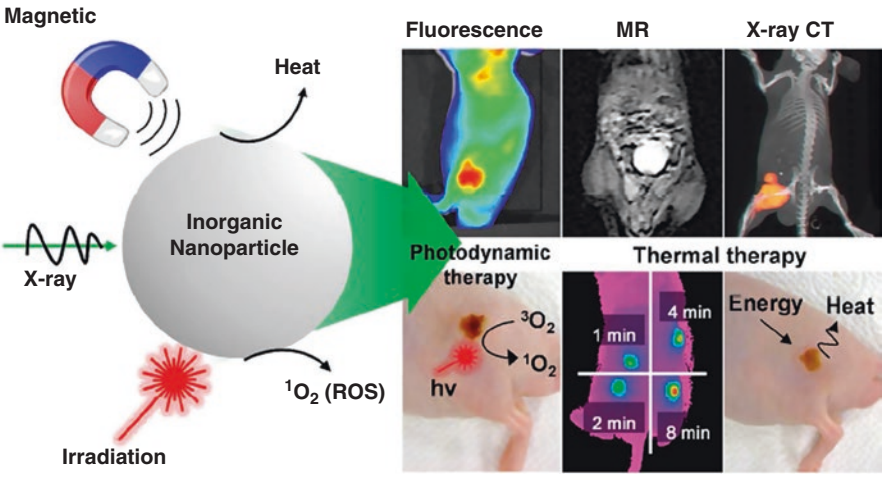

Fig. 5.1 Inorganic nanoparticles for tumor imaging and therapy. Reprinted with permission from [12]. Copyright © 2016 American Chemical Society

energy transfer, X-ray absorption, and properties, inorganic nanoparticles are favorable choice for image guided therapy (IGT) as well as in bio-imaging.

5.2.1.1 Fluorescence-Based Imaging

Since long time, the fluorescence-based nanoparticles have been using for imaging of various cells, tissues, organs, etc. for the biomedical applications which advanced the current labeling technology. Dyes such as indocyanine green and fluorescein are conventionally used. Fluorescence detection method generally depends on either emission from externally administered markers (fluorescent) or the autofluorescence of the tissues coming from different concentrations of the fluorophores (endogenous) or fluorescent materials induced [13, 14]. For example, Lai et al. prepared FRET (fluorescence resonance energy transfer) based monitoring system (real) which consisted four components, a) mesoporous silica nanoparticles for drug carrier which was further labeled with coumarin (donor); b) FITC (acceptor) attached beta cyclodextrin in order to trap the drugs inside the nanoparticles; c) to release the drug molecule in a redox-responsive manner through disulfide linkage; d) coumarin and FITC as FRET donor-acceptor pair for observing the drug release [15]. The authors observed that under non-reducing conditions the disulfide bond was intact that assisted the FRET between coumarin (donor) and FITC (acceptor). The close proximity of both the donor and acceptor helped the process. The group showed that in presence of glutathione (GSH), no FRET was observed between donor and acceptor because of the breakage of disulfide bond. This process helped in the drug release from the nanoparticles. The group mentioned that the donor-acceptor pair could operate the drug release process by changing the FRET signal in real time. On the other hand, Nakamura et al. prepared fluorescent organosilica nanoparticles coated with PEG by one-step process for bio-imaging [16]. The group

evaluated the stealth function of the nanoparticles by observing the kinetics, patterns, and uptake of these nanoparticles using flow cytometry analysis and single cells time-lapse microscopic imaging. Additionally, they observed that stealth function was not observed in case of PEG-insensitive macrophages, whereas it mostly observed in PEG-sensitive macrophages. Finally, the interaction of the nanoparticles with the immune cells helped in understanding the accelerated blood clearance (ABC) phenomenon. Not only the silica-based nanoparticles, but also the carbon dots are used as fluorescent-based imaging probes. For example, Bhunia et al. chemically synthesized the carbon dot nanoparticles (size within 1–10 nm) for cell imaging that exerted tunable emission in the visible region (blue to red) in a size dependent manner [17]. They further modified these nanoparticles by surface functionalization for cell imaging probes. Altogether, the authors concluded that these non-toxic carbon dot nanoparticles could be used as an alternative to toxic nanoparticles (cadmium based) useful for biomedical applications. In another example, Li et al. used the next generation optical imaging method for noninvasive imaging of tumor metastasis and vessel by near infrared emission (beyond 1500 nm) that showed high sensitivity and resolution (spatial) [18]. The group prepared polyacrylic acid (PAA)-modified $NaLnF_4$:40Gd/20Yb/2Er nanorods (Ln = Y, Yb, Lu, PAA-Ln-NRs) having downshifted NIR-IIb emission. To validate its applicability, the PAA-Lu-NRs were used in cancer therapy for small tumor detection in Lewis lung carcinoma (LLC) tumor-bearing mouse model. The schematic representation of the small tumor diagnosis in vivo model was carried out using PAA-Lu-NRs as shown in Fig. 5.2a. The PAA-Lu-NRs were intravenously injected inside the tumor-bearing mouse and images were captured at various time points (1–60 h) as shown in Fig. 5.2b. At 1 h time point, the signals were mainly observed in spleen and liver. After 24 h the signals were found in the tumor site and significantly increased upto 48 h, indicating the feasible application of the PAA-Lu-NRs as shown in Fig. 5.2b. The bright NIR-IIb emission was observed in the spleen, liver, lung, and tumor site of the mouse which corroborated the distribution trend in living mouse as shown in Fig. 5.2c-d. Finally, the group concluded that the low toxicity, high quantum yield, size uniformity, and narrow band emission capability made the nanoparticles useful candidate for multimodal imaging.

5.2.1.2 Photoacoustic Imaging

Among different optical imaging techniques, the photoacoustic imaging has got immense attention. It is generally based on the thermoelastic expansion of the tissue after illuminating with the pulsed laser light, resulting in absorption of energy as well as generation of heat. Actually, PAI (photoacoustic imaging) binds both the properties of ultrasound imaging (the high penetration depth, sensitivity) along with the pulsed laser light illumination (multispectral possibilities) [19, 20]. PAI is used in various areas in biomedical applications such as vascularization, for detection and monitoring of tumors, lymph nodes (sentinel), etc. [21–23]. Recently, several nanoparticles are employed such as gold [24], polymeric nanoparticles [25], carbon nanotubes [26], etc. for PAI [19]. For example, Wu et al. applied green synthetic approach for the synthesis of carbon nanoparticles from honey for photoacoustic

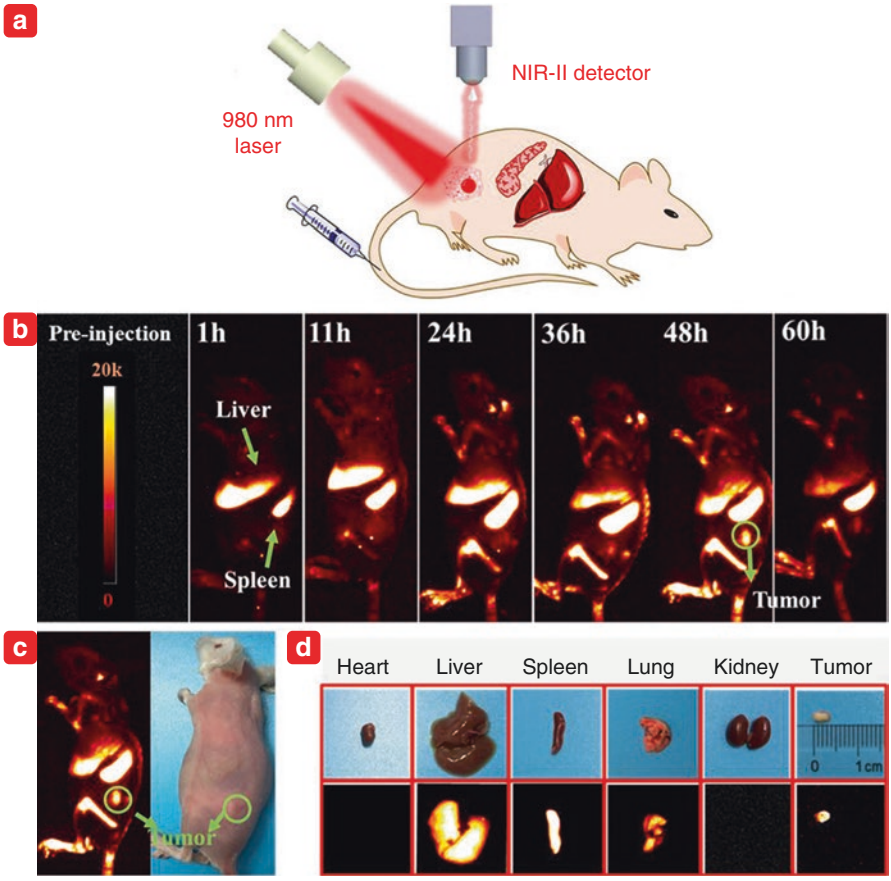

Fig. 5.2 (**a**) Schematic illustration of in vivo small tumor diagnosis by using PAA-Lu-NRs. (**b**) NIR-IIb bio-imaging of LLC tumor-bearing mouse after intravenously injecting PAA-Lu-NRs at different time periods. (**c**) Digital photograph of tumor-bearing mouse and in vivo NIR-IIb fluorescent imaging of the tumor-bearing mouse (the green circle indicated the tumor site). (**d**) Digital photographs of the isolated organs/tumor and the corresponding ex-vivo NIR-IIb imaging, respectively. Reprinted with permission from [18]. Copyright © 2019 American Chemical Society

imaging (real time). Researchers used the solvent-free condition for surface modification of those carbon nanoparticles with organic macromolecules [27]. Figure 5.3 shows the PA (photoacoustic) imaging of SLN (sentinel lymph node) in nude mice at 650 nm laser. At different time point, images were captured: (1) before OCN (luminescent carbon nanoparticles) injection, (2) after 2 min, (3) 210 min of postinjection. Blood vessels, SLN, and lymph vessel were clearly visible after 2 min of injection. The PA control images before OCN injection referred as maximum intensity projections (MAP). The enhancement of PA was observed 51 times in case of SLN after 2 min of injection. The group revealed that after 210 min postinjection, the contrast of the PA images decreased owing to rapid clearance of the particles

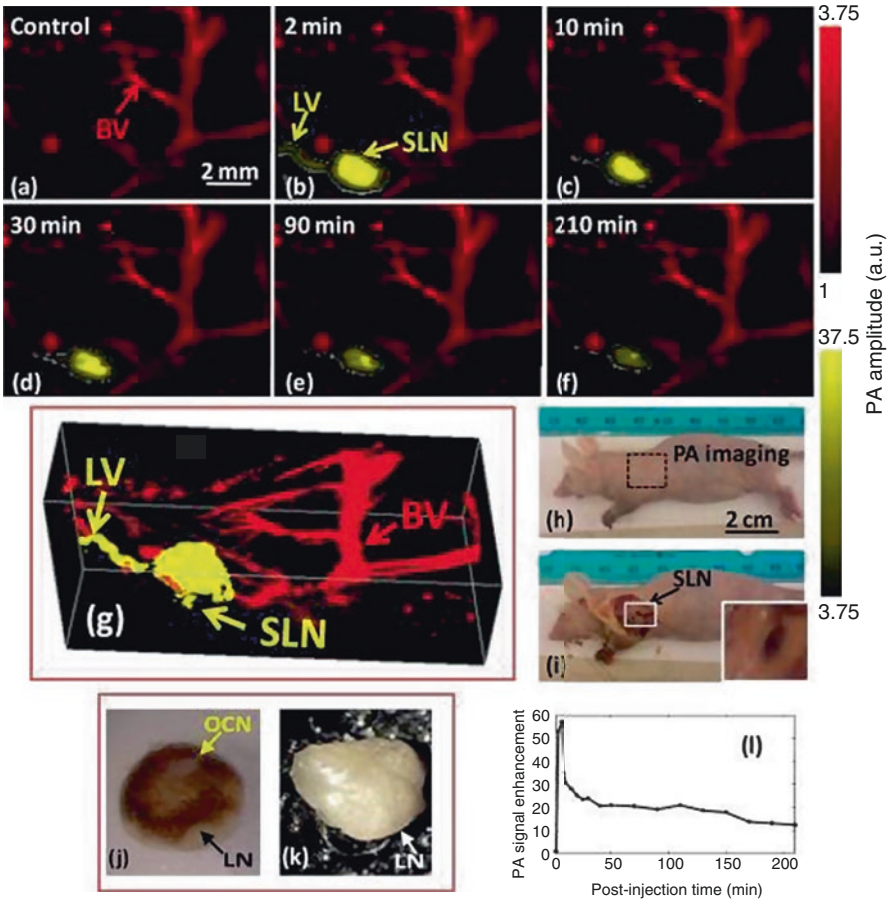

Fig. 5.3 Noninvasive real-time in vivo PA imaging of SLN in nude mouse: For all PA images, the laser was tuned to 650 nm wavelength. (**a**) Control PA image acquired before OCN injection. Red parts represent optical absorption from blood vessels (BV); (**b**) PA image acquired immediately (2 min) after the OCN injection; blood vessel (BV), lymph vessel (LV), and sentinel lymph node are marked with arrows, and the SLN is visible in (**b**–**e**); however, the contrast is much weaker after 210 min postinjection in (**f**). (**g**) 3D depiction of the SLN and BVs immediately after OCN particles injection, (**h**) Photograph of the nude mouse before taking the PA images. The scanning region is marked with a black dotted square. (**i**) Photograph of the mouse with the skin removed after PA imaging, accumulation of dark-colored OCN particles is visible in lymph node; (**j**) excised and isolated lymph node from mouse injected with OCN after 0.5 h and (**k**) injected with saline; (**l**) PA signal enhancement in the SLN after the injection of OCN nanoparticle as a function of postinjection time. For (**a**–**d**): FOV = 12 mm × 10 mm, step size along the X direction = 40 μm, step size along the Y direction = 100 μm, raster scanning for a 3D image = ~1 min, B-scan frame rate = ~1.5 Hz, total scan time = ~210 min. No signal averaging was used. Reprinted with permission from [27]. Copyright © 2019 Elsevier B.V

from lymph node. The nude mice were photographed before and after PA images. No dark color was found in case of saline-treated nude mice, whereas OCN-treated nude mice demonstrated dark color accumulation of the nanoparticles. The group revealed that there was a huge increment in the PA signal after injection which went away in a time dependent manner. On another example, Kricher et al. designed nanoparticles consisting of gold core useful for PAI, outer layer for SERS (surface-enhanced Raman spectroscopy) along with a gadolinium-based layer for MRI [28]. Researchers employed this kind of MPR (magnetic resonance-photoacoustic-Raman) nanoparticles to identify the tumors using MRI. Additionally, the deep-seated tumor was localized using PAI and the fine margin re-sectioning was carried out using SERS. Finally, the authors shed lights on the future applicability of this PAI as noninvasive techniques by making it more clinically effective tools for imaging. Apart from that, advanced PAI setups were enabled for the differentiation of the background signals from the probe-specific signals. In this context, multispectral optoacoustic tomography (MSOT) is used for the quantitative assessment of the exogenous (porphyrin, methylene blue, etc.) and endogenous (hemoglobin, melanin, etc.) contrasting agents [29] [30]. Meanwhile, in order to visualize the gastrointestinal cancer, PEGylated gold nanoparticles were successfully employed in MOST as signal amplifiers. Similarly, to specifically target the integrin $\alpha_v\beta_3$ (overexpressed in tumor neovasculature), RGD peptide conjugated gold nanoparticles were prepared for PAI useful for sensitive angiography [31].

5.2.1.3 Raman Based Imaging

Raman based imaging is a powerful, noninvasive, label-free imaging technique used for the study in different chemical processes in biology [32].The in-elastic scattering of the light (photon) from a particular object gives rise to Raman effect. It can be performed in robust conditions and useful in providing the molecular details, fingerprints of tissues, cells, etc. For example, Lu et al. developed gold nanopopcorn functionalized with RNA aptamers and incubated in cancerous as well as non-cancerous cells for imaging [33]. The authors showed that the central AuNP (gold nanoparticle denoted as "popcorn") acted as electron reservoir, whereas the surrounding AuNPs focused the Raman field at the apexes. The group demonstrated that in the cancer cells, the aggregated nanoparticles formed "hot spots" and promoted surface-enhanced Raman scattering (SERS) imaging. Additionally, they observed that Raman signal enhancement property differentiated the cancer cells and normal cells. Finally, the authors concluded that this system could be used for early diagnosis of cancer cells using Raman spectroscopy. Generally, Raman spectroscopy does not depend on the endogenous fluorophores and local environment. Over the years, variants of Raman spectroscopy are explored to increase the sensitivity and to address the problems of continuous Raman scattering. This new type of imaging technique [Coherent anti-Stokes Raman scattering (CARS)] can improve vibrational signals and has high speed video rate imaging capacity. Monger et al. used this noninvasive technique in order to locate the metal oxide nanoparticles [cerium dioxide (CeO2), zinc oxide (ZnO-NP), and titanium oxide (TiO2-NP)] in gills of *Oncorhynchus mykiss* (rainbow trout) [34]. The authors observed the

structures of the lamella in the gills after H and E staining using CARS techniques. In addition, the group explained that the carbon- and hydrogen-rich structures depicted the high strain uptake areas as observed by the CARS images. Also, they detected the various sizes nanoparticles in the agarose gel and found aggregated nanoparticles applying the Forward CARS. Small size nanoparticles were not observed because of the reduction of the Forward CARS signal. Researchers showed that small aggregated nanoparticles of TiO_2 generally located in the periphery of the lamella for short time exposure, whereas under long exposure period the large aggregated particles were found inside the secondary lamella [35]. In another example, the uptake of PLGA [poly (lactic-co glycolic acid)] nanoparticles loaded with C6-ceramide-d_{11} drug for targeting the epidermal growth factor receptor in SKOV3 cell was observed [36]. The uptake of the growth factor targeted nanoparticles in the SKOV3 cells was observed after 2 h as shown in Fig. 5.4a. The non-targeted nanoparticles did not enter the cells upto 6 h. The authors mentioned that the cell body, nucleus (blue), endocytic vesicle (yellow), membrane organelles (green), and the red colored nanoparticles were visible by applying the vertex component analysis. The group demonstrated that overlaid of these components showed the nanoparticles distribution in the cell. In another study, inside the PLGA nanoparticles beta-carotene was encapsulated and the nanoparticles were incubated in NIH-3T3

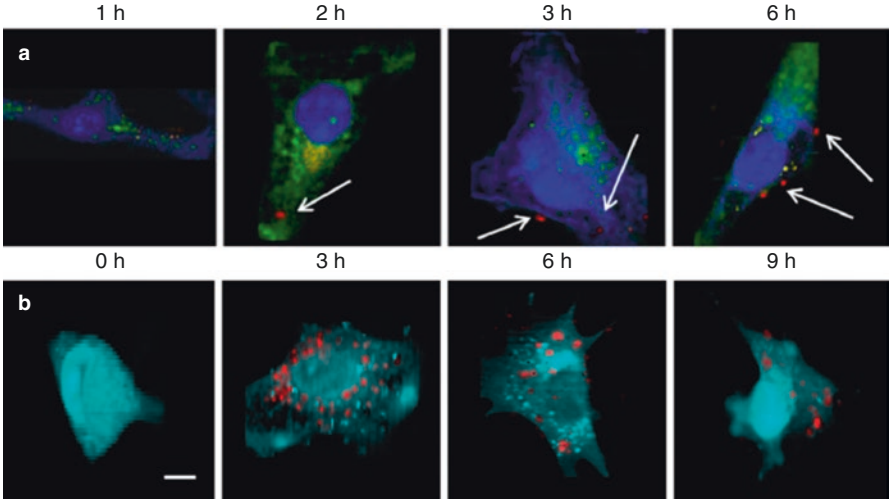

Fig. 5.4 The uptake of polymeric nanocarriers. (**a**) The uptake of epidermal growth factor receptor targeted nanoparticles to SKOV-3 cells over time shows that particles enter after 2 h. Images are overlays of the cell body and nucleus (blue), membranous organelles (green), early endocytic vesicles (yellow), and nanoparticles (red). White arrows show regions of nanoparticle aggregation. Reproduced with permission from [82], published by Springer Nature (2013). (**b**) The uptake of β-carotene-loaded poly lactic-co-glycolic acid (PLGA) nanoparticles into murine NIH-3T3 cells showing the cell body (cyan) and nanoparticles (red). Scale bar = 10 μm. Reproduced with permission from [83], Copyright John Wiley. Reprinted with permission from [36]. Copyright © 1996–2019 MDPI (Basel, Switzerland)

cells (mouse fibroblast) [36]. The presence of the double bonds (conjugated) and the extended vibrational structure indicated the possibility of resonance Raman spectroscopy at a discrete wavenumber. Researchers observed that there were discrete strong bands which are unique to the beta-carotene. The uptake of the nanoparticles at different time points were shown in Fig. 5.4b, in which the cell body was observed in cyan and the nanoparticles were in red.

5.2.1.4 MRI-Assisted Imaging

MRI imaging is based on nuclear magnetic resonance principle in which the hydrogen nuclei absorb radiofrequency pulses of the resonant and get excited in presence of strong magnetic field [37]. The excited nuclei then returned back to the ground state after emission of the absorbed radiofrequency. The different relaxation characteristics of the hydrogen atom in presence of magnetic fields give contrast to the MRI. It has been observed that paramagnetic materials increase the longitudinal relaxation (T1 relaxation) resulting to brighter signals, whereas ferromagnetic as well as superparamagnetic materials give rise to transverse relaxation (T2 relaxation) producing hypointense signal. Based on the concept, the gadolinium (Gd^{3+})-based and superparamagnetic iron oxide materials are used as contrasting agents [38]. Earlier, T2 contrast imaging agent Feridex and Resovist (first generation) and Combidex (second generation) were used to detect liver lesions, but they became obsolete from the market owing to more usefulness of T1 contrast images [39]. There are various side effects of gadolinium-based agents like nephrogenic systemic fibrosis, whereas the iron oxide nanoparticles are typically degraded in liver and spleen and entered into the iron metabolism when injected intravenously [40, 41]. According to reports, the iron oxide nanoparticles are useful in MRI of gastrointestinal tract when administered orally. Additionally, the controlled size, tunable magnetic property, crystalline nanoparticles can be obtained by synthesizing the nanoparticles based on their thermal decomposition. This alteration in the synthesis process results as an alternative to T1 contrast agents such as Gd (III) based along with the T2 contrast agents which are highly sensitive. For example, ESIONs (extremely small iron oxide nanoparticles) with size around 3 nm exerted high T1 contrast effect [42]. In another example, good T2 contrast effects were observed from the 30 nm sized iron oxide nanoparticles owing to the facile cellular uptake of the nanoparticles [43]. Also, it has been observed that 22 nm iron oxide nanoparticles gave rise to stronger contrast effects attributed from the balanced magnetization as well as diffusion rate predicted by the outer-sphere relaxation theory [44]. Furthermore, the surface modification of the nanoparticles, attachment of targeting ligands (aptamer, folic acids, etc.), and functional molecules (fluorescent dyes) potentiate the nanoparticles-based MRI contrast agents. Meanwhile, in order to overcome the intrinsic drawbacks of MRI itself such as artifact signals, hypointensity, or hyperintensity owing to the endogenous factors like fat, bleeding, metal deposition, etc., the dual mode contrasting agents (T1–T2) came into action [45]. This system contained superparamagnetic nanoparticles along with paramagnetic metal ions to provide better contrast. Apart from that, clustering of the nanoparticles also creates problem by changing the T2 relaxation rate known as magnetic

relaxation switch (MRS). Ling et al. reported an iron oxide nanoparticle which can activate the MR signals in acidic environment because of the presence of the pH responsive polymer surrounding it [46]. The authors observed that appearance of strong T2 contrast effects retards the T1 contrasting effects in aggregated form. Additionally, disassemble of the nanoparticles augmented T1 weighed MRI signal in acidic condition. Other than the iron-based nanoparticles, lanthanide-based nanoparticles hold superior position as MRI contrast agents. For example, $NaGdF_4$ nanoparticles are used for T1 weighed MRI. Holmium-based, dysprosium-based nanoparticles also got much attention due to their large magnetic moment along with short relaxation time beneficial for high field MRI [47, 48].

5.2.1.5 CT Imaging

CT (computed tomography) imaging is a kind of whole-body imaging system which has been widely used because of its high resolution as well as rapid acquisition power [49]. It is based on the principle of the X-ray interaction with the contrasting agents or body. The intensity of the X-ray generally measures from different angles using computer, which captures the crosssectional images (tomographic) produced due to the rotation of the detector and the X-ray tube. It is used to visualize organs like brain, lung, gastrointestinal tract, abdominal portion as well as cardiovascular system, etc. As the X-ray depletion property increases with increasing the atomic number, high Z value is preferable option as CT contrast agents. In the clinical situations, iodine-based and barium-based contrasting agents are in use till date [50, 51]. Since high dose is required for CT scan, toxicity of the materials is major concern. Barium sulfate suspension which has been used for long time for gastrointestinal imaging showed renal and cardiovascular toxicity when administered in intra-vascular route. On the other hand, iodine-based molecules such as iodixanol and iopamidol were FDA approved for intravenous CT contrast agents. The induction of allergic reactions, lower blood circulation time as well as renal toxicity is major drawbacks [50, 52]. Last but not least, the gold-based CT contrasting agents are a great alternative than that of iodinated agents because of its easy synthesis along its biocompatible nature. For example, Reuveni et al. injected the gold nanoparticles conjugated with anti-epidermal growth factor receptor into the nude mice which were implanted with human squamous cell carcinoma (SCC) head and neck cancer [53]. Figure 5.5 shows the volume-rendered images of mouse under X-ray computed tomography before injection with gold nanoparticles, postinjection after 6 h with IgG-coated gold nanoparticles and the anti-epidermal growth factor receptor targeted gold nanoparticles. The group observed that CT number of the tumor targeted by the anti-epidermal growth factor receptor conjugated gold nanoparticles was much higher than that of only gold nanoparticles injection, which clearly showed that the attachment of the nanoparticles with the SCC head and neck tumor resulted in high contrast effects. Finally, the authors shed lights on the future applicability of this imaging technique for the detection of smallest tumors possible. According to reports, almost 50 gm gold is required for each whole-body scanning which makes it difficult to use in terms of cost. So, lanthanide metal such as Ytterbium (Yb) can be a good alternative. But, the large-scale production of

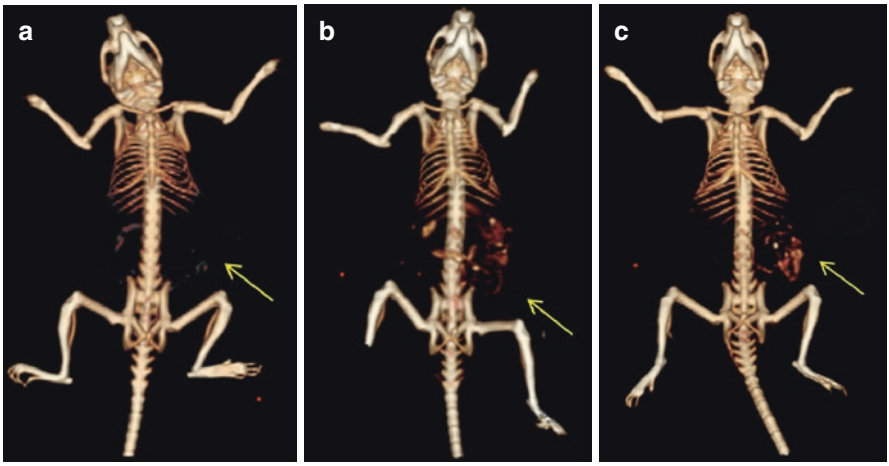

Fig. 5.5 In vivo X-ray computed tomography (CT) volume-rendered images of (**a**) mouse before injection of gold nanoparticles (GNPs), (**b**) mouse 6 hours postinjection of nonspecific immunoglobulin G GNPs as a passive targeting experiment, and (**c**) mouse 6 hours postinjection of anti-epidermal growth factor receptor (EGFR)-coated GNPs that specifically targeted the squamous cell carcinoma head and neck tumor. The anti-EGFR-targeted GNPs show clear contrast enhancement of the tumor (**c**, yellow arrow), which was undetectable without the GNPs contrast agents (**a**, yellow arrow). CT numbers represent the average Hounsfield units (HU) of the whole tumor area. All scans were performed using a clinical CT at 80 kVp, 500 mAs, collimation 0.625 × 64 mm, and 0.521 pitch size (64 detector CT scanner, LightSpeed VCT; GE Healthcare, Little Chalfont, UK). Reprinted with permission from [53]. Copyright © 2019, Dove Press Ltd.

lanthanide is a problem in order to utilize it as CT contrast agents. Even though the radiation dose is high in case of CT, the vast availability and fast scanning speed make it the most useful imaging tools [54–56]. Meanwhile the usage of the contrasting agents arises conspicuity of the images, necessary action can be taken on the administered dosage to reduce the radiation exposure resulting in safer imaging. Also, the toxicity evaluation of the nanoparticles is urgently needed, for successful translocation of the nanoparticles into clinical trials.

5.2.1.6 Multiphoton Microscopy Imaging

Now-a-days, the multiphoton imaging system has got paramount importance because of their several advantages over whole-body imaging techniques like MRI and CT scan [57, 58]. The multiphoton imaging system is a kind of anti-strokes emission that creates shorter emission wavelength compared to wavelength of excitation [59]. It is well known that it reduces the photobleaching of fluorophores as well as decreases the damages of sample after photoinduction. Additionally, in combination with infrared, this multiphoton fluorescence imaging system can minimize the background autofluorescence and improve penetration depth [60]. But, most of the multiphoton imaging dyes consist of small molecule; they are in general less photostable which prohibit them for prolonged imaging and frequent excitation.

Hence, metal nanoparticles-based multiphoton imaging probes are in good demand owing to their ease surface modification, fictionalization and reduced photobleaching capability. Among various nanoparticles, quantum dots (QDs) are well studied in this area because of their tunable emission and broad multiphoton cross sections [61]. In this context, quantum dots containing cadmium such as CdSe/CdS/ZnS nanoparticles (two-photon imaging system) were studied which showed potential toxicity. To address this toxicity issue, manganese doped ZnS nanoparticles (ZnS:Mn) (three-photon imaging probes) have been used owing to their larger absorption cross sections [62]. Despite their low toxicity value, they can penetrate deep as well as enable more light to escape from the tissue. Simultaneously, this system decreases the background fluorescence, the out of focus excitation and automatically escalates the spatial resolutions. Other than the ZnS:Mn quantum dots, there are other QDs which are well known for their non-toxic nature such as $CuInS_2$/ZnS, etc. [63]. Meanwhile, the light scattering from biological tissue creates additional problem during fluorescence imaging by using three-photon system that uses NIR laser. To overcome the pitfalls, and to decrease the light scattering, it has been taken into account that the three-photon system can be excited at second NIR-II range (1000–1700 nm) to get better efficacy [64]. It has been observed that in the ZnS:Mn system, the excitation of the manganese dopant at 1050–1310 nm light source is more beneficial than excitation of the ZnS host at 600 nm laser because of the vast two-photon cross sections of manganese ions which improves penetration depth. Apart from that, there are several issues that need to take care to get a high-resolution image in quick acquisition time using multiphoton imaging system.

5.2.1.7 Super Resolution Methods in Optical Microscopy

Super resolution methods for optical imaging have got immense attention after the breakthrough invention of "Super resolved fluorescence microscopy" by Eric Betzig, Stefan W. Hell, and William E. Moerner, those who got the noble prize in 2014 in chemistry [65, 66]. Since then, it has become a very captivating field in the science. In 2014, Zhu et al. prepared biodegradable SP-PCL [spiropyran-terminated poly(ε-caprolactone)] nanoparticles using Tetra spiropyran titanate [$Ti(SP)_4$] as precursor [67]. The authors explained that upon UV irradiation the SP-PCL exhibited photochromism owing to the transformation of SPs into merocyanines (MCs). The group observed that upon excitation at 420 nm, the SP-PCL and MC-PCL exerted emission at green (530 nm) and red region (650 nm), respectively. The group found out that owing to interconversion of both the forms (SP- and MC-), SP-PCL nanoparticles showcased both the green and red fluorescence. The authors declared that this biodegradable SP-PCL nanoparticle acted as potential candidate as fluorophores (photoswitchable) in super resolution microscopy (localization based) in order to visualize sub-cellular nanostructures which is higher than normal fluorescence microscopy. On the other hand, Lin et al. observed that in order to detect the surface-enhanced fluorescence (SEF) on metal nanostructures, photoactivation localization microscopy (PALM) have been studied well [68].

5.2.1.8 Luminescence Upconversion Imaging

Recently, the upconversion imaging probes have got huge attention in the field of imaging owing to the longer luminescence lifetime and newly developed luminescent probes. Upconversion generally follows a kind of anti-stokes mechanism, where the photon absorption process occurs through intermediate electronic states (real) [69]. Compared to multiphoton absorption, this imaging system provides much higher emission frequency [70]. It has been observed that for the lanthanide doped upconversion nanoparticles (UCNPs), it is possible to tune the emission color by simply changing the composition of the elements due to dependency on the energy levels of each elements other than its quantum confinement [71, 72]. Other advantages observed in case of lanthanides that the lifetime (luminescence) can also be adjustable several folds (microseconds) useful for multiplex imaging by using different types as well as the changing dopant percentages [70]. These UCNPs are also useful for time-gated fluorescence imaging due to segregation of light scattering from the nanoparticles emission which give rise to better contrast [73]. According to reports, the lanthanide doped UCNPs exceeded the popularity of organic-based materials owing to the triplet-triplet annihilated upconversion along with enhanced photon collection efficacy arising from functionalization with antenna materials (NIR dyes, QDs, etc.). Besides, they have extreme photostability and chemical stability [74, 75]. Apart from that, there are several limitations associated with these luminescence upconversion nanoparticles. First of all, owing to the ladder like energy levels, multiple emission peaks appear in case of lanthanide doped NPs. Thallium generates peaks at NIR, UV, blue region; erbium gives both red and green emission [76]. Secondly, the heating effect of the laser (980 nm NIR) is used in case of UCNPs, which can increase the temperature of the water molecules rendering problems to the imaging techniques. It can cause the damage to the tissue during in vivo imaging. To overcome this problem, Xie et al. introduced the Nd^{3+}(ions) in the system that used laser (800 nm) with moderate heating [77]. The used laser can be absorbed minimally by water which ultimately solved the heating issue. The group mentioned that Nd^{3+} ions acted as sensitized dopant in this system. They illustrated the idea of the core–shell strategy that precisely described the control over the ions (acted as dopant) in forming the core and shell layers of nanoparticles in Fig. 5.6a. The authors demonstrated that the less amount of Nd^{3+} doping as a core led to less concentration quenching, whereas high amount of doping in the shell layer carried out for effective harvesting of light (~800 nm). Researchers observed that the absorption intensity was much higher in case of Nd^{3+} doping (shell layer) compared to control (no Nd^{3+} doping in the shell layer) at 794 nm as shown in Fig. 5.6a. They also found that there was significant difference in the absorption intensity of the Nd^{3+} doped (shell layer) and the Yb^{3+} doped (core) at 794 nm and 976 nm, respectively. The Nd^{3+} doped (shell layer) demonstrated remarkable increase in intensity compared to Yb^{3+} doped (core) nanoparticles. The absorption spectra of the system were normalized at 976 nm as shown in Fig. 5.6b. Meanwhile, there are various applications of these UCNPs observed in in vivo system. Park et al. used Tm^{3+}-doped UCNPs for optical imaging and trafficking of nanoparticles in lymphatic system

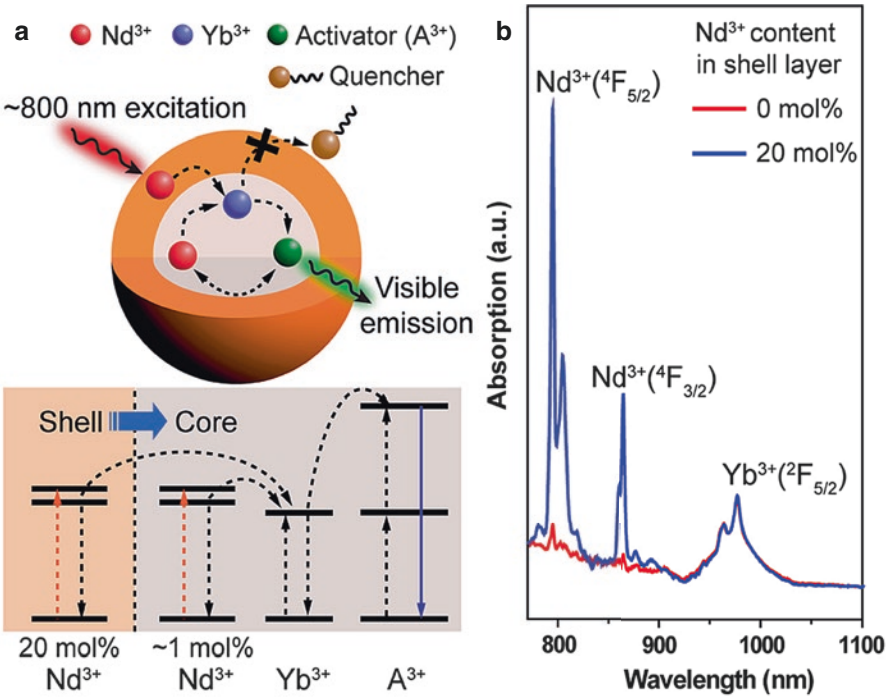

Fig. 5.6 (**a**) Schematic design (top) and simplified energy level diagram (bottom) of a core–shell nanoparticle for photon upconversion under 800 nm excitation. Nd3+ ions doped in the core and shell layers serve as sensitizers to absorb the excitation energy and subsequently transfer it to Yb3+ ions. After energy migration from the Yb^{3+} ions to activator ions, activator emission is achieved via the Nd3 + −sensitization process. (**b**) Near-IR absorption spectra of NaYF4:Yb/Nd(30/1%) nanoparticles coated with an inert NaYF4 shell or an active NaYF4:Nd(20%) shell. The absorption spectra were normalized at 976 nm for comparison. Reprinted with permission from [77]. Copyright © 2013 American Chemical Society

of mice [78]. Researchers mentioned that this high advanced NIR-NIR upconversion luminescence (UCL) provided the luminescence profiles in SLN (sentinel lymph node) tissues, organs, etc. even in feaces of mice for over one month studying time. Additionally, the group observed the clearance of the injected NPs through hepatobiliary site evincing from the flowing of the NPs rapidly via lymph node to the main blood stream. Finally, the authors shaded lights on the future applicability of the UCNPs in immunology along with biopsy analysis in SLN. Another study laid by Jayakumar and co-workers, where they used this UCNPs (silica-coated nanocrystals) in order to study the gene expression in zebrafish model proved to be a game changer in this field [79]. The silica-coated Ytterbium, Yttrium, and Thulium (lanthanide elements) exerted UV light when activated by the NIR light resulting in the photoactivation in deep tissue. The authors described that the knockdown of the notochord creator and mesoderm modulating gene (−ntl) was light guided. In the adult zebrafish model, the

knockdown was guided through GFP transplanted tumor cells using NIR light. Additionally, the embryos as well as the adult zebrafish were imaged which gave future direction of potential use of this system in development of biologics.

5.2.2 Image Guided Disease Therapy Using Nanoparticles

The major challenges of cancer including early detection, limitations of chemotherapeutic agents, and continuous monitoring of metastatic cancer cells require a strategy in order to visualize as well as fight against them. Therefore, nanotechnology-based approaches are emerging as vital platforms for disease diagnosis and therapy. Image guided disease therapy means simultaneous imaging and therapy of the disease which is a combined approach to understand the localization of therapeutic molecules in real time. This strategy also enables in estimating the therapeutic effect of the nanoconjugates in the body by imaging the tumor volume [80]. Nanotechnology offers conjugation of imaging molecules (fluorescent agents, MRI contrast agents, etc.) and therapeutic molecules together in order to visualize the tumor and also for treatment [81]. Various research groups have practicing in the development of such kind approaches using different types of nanomaterials. Among all, iron nanoparticles are widely employed for the image guided therapy. For example, Yu et al. developed nanotheranostic approach for prostate cancer therapy [82]. The authors designed thermally cross-linked superparamagnetic iron oxide nanoparticles (TCL-SPIONs) conjugated with aptamer which is specific ligand for prostate-specific membrane antigen (PSMA) and loaded with doxorubicin as anticancer agent. The Apt-hybr-TCL-SPION nanoconjugate exhibited the tumor-specific uptake in LNCaP xenograft mouse model. The study explained dual role of iron oxide nanoparticles for imaging and therapy of prostate cancer. Similarly, Tomitaka et al. synthesized magnetic core/gold shell (MNP@Au) magneto-plasmonic nanoparticles for MRI imaging of brain diseases [83]. The as-synthesized nanoparticles displayed superparamagnetic properties and MRI contrast applications. Further, magneto-plasmonic nanoparticles could be able to cross the BBB (blood–brain barrier) as confirmed by transmigration study *in vitro*. Considering these observations, the authors claimed that magneto-plasmonic nanoparticles help in treatment of neurological disease. On the other hand, Satpathy et al. developed amphiphilic polymer iron oxide nanoparticles conjugated with HER2 affibody labeled with NIR dye as targeted agent and cisplatin as chemotherapeutic agent [84]. The study demonstrated that iron oxide nanoparticles significantly suppressed the primary and metastatic ovarian tumor growth observed in xenograft mice model. Duc et al. developed Gadolinium based-nanoparticles (GBNs) for image guided radiation therapy for brain tumors [85]. The group stated that the GBNs were able to induce MRI contrast and radiosensitizing effect. The GBNs were activated by X-ray microbeams to kill the brain cancer cells resulted in increased lifespan of rats bearing the brain tumors.

Gold nanoparticles (AuNPs) are also widely employed for the image guided therapy. Due to their unique photonic properties, AuNPs are employed as optical contrast agents [86]. Optical coherence tomography (OCT) and photoacoustic (PA)

imaging are the two important imaging modalities which employs the light scattering or absorption properties of AuNPs [87]. For example, Etame et al. demonstrated the magnetic resonance-guided focused ultrasound (MRgFUS) using AuNPs to deliver therapeutic agents for central nervous system (CNS) [88]. The authors found that AuNPs were able to deliver the therapeutic agents into CNS in presence of focused ultrasound. Similarly, Gao et al. nicely described the image guided therapy using AuNPs with graphene oxide (GO) [86].The AuNPs were seeded on to GO to form GO/Au complex which was conjugated with Cy5.5 labeled-matrix metalloproteinase-14 (MMP-14) substrate (CP) [CPGA: final conjugate]. The CPGA exhibited the high fluorescent and PA signals in the mice bearing the SCC7 tumor and able to inhibit the tumor growth upon irradiation using laser.

5.2.3 Biosynthesized Nanoparticles for Bio-imaging

In recent times, biosynthesized nanoparticles are also employed for bio-imaging applications. For instance, our group for the first time demonstrated the bio-imaging applications of biosynthesized nanoparticles silver:b-AgNPs prepared by *Olax scandens* leaf extract [89]. We observed that the *Olax scandens* plant contains different phytochemicals attached to the nanoparticles during the synthesis (in situ) which could be used for fluorescence-based bio-imaging. The b-AgNPs displayed the red color fluorescence upon administration in A549 cells [89, 90]. UT or control cells did not show any fluorescence (Fig. 5.7a). The only leaf extract showed less fluorescence due to lesser uptake by the cells as shown in Fig. 5.7b. Similarly, the b-AgNPs exhibited the red color fluorescence in B16F10 cells, whereas the chemically synthesized silver nanoparticles (c-AgNPs) did not show any fluorescence inside the cells as shown in Fig. 5.7c-d, respectively. The phase contrast images of various treatment groups and control cells are shown in Fig. 5.7a'-d'. Interestingly, the normal cells did not show the fluorescence color. However, this cancer cell specific property of these biosynthesized silver nanoparticles is yet to understand. The bio-imaging properties of biosynthesized nanoparticles show the future directions to develop the plant-based fluorescence molecules towards biomedical applications.

5.3 Clinical Status of Nanoparticles-Based Bio-imaging

Presently, various nanoparticle-based imaging agents are approved for clinical uses which by FDA or some in clinical trials. For example, definity is an FDA approved perflutren lipid microspheres used as ultrasound contrast agents [91].These microspheres are the lipid microspheres filled with gas which reflect the sound waves to provide the better contrast picture. Generally, these microspheres are administered through intravenous injection for the diagnosis of heart diseases. Similarly, Optison (GE Healthcare) is also another contrast agent approved by FDA which is a human serum albumin stabilized perflutren microspheres [91]. Further, ferumoxytol is

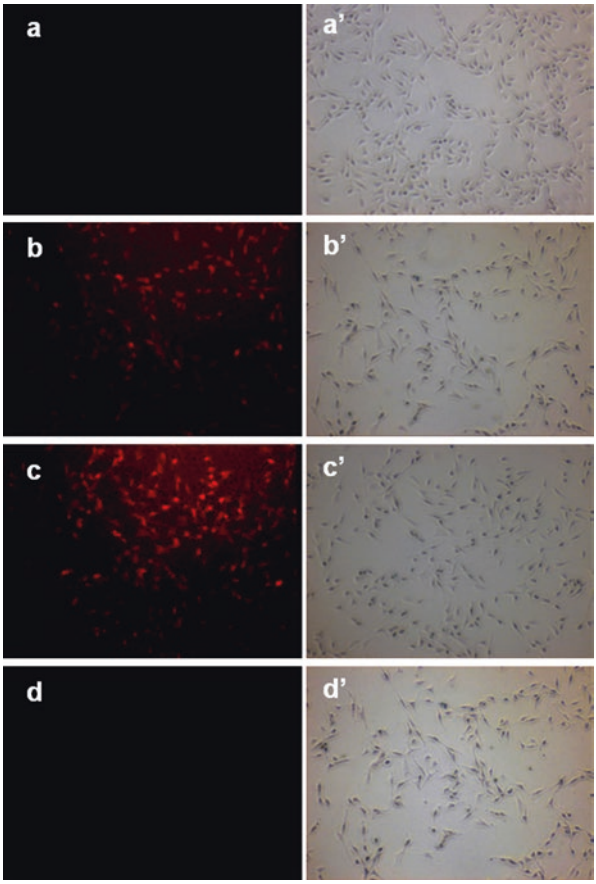

Fig. 5.7 Fluorescence and the corresponding phase images of untreated B16 cells and cells treated with Olax, b-AgNPs, and c-AgNPs, observed by an Olympus Fluorescence Microscope. Fluorescence images of B16 cells treated with (**a**) untreated or control, (**b**) Olax (100 µg/ml) leaf extract, (**c**) b-AgNPs (at 30 µM), and (**d**) c-AgNPs (at 30 µM). Images of a', b', c', and d' correspond to phase images. All the treated B16 cells were extensively washed with DPBS (6 times) before taking the fluorescence images. It is to be noted that there is no significant cell killing observed at 30 µM. Reprinted with permission from [89]. Copyright ©2019 Ivyspring International Publisher

another FDA-approved imaging agent for off-label as MRI angiography agent as well as for iron deficiency anemia [92]. AuNPs-based formulations are also approved by FDA for diagnosis applications. For instance, Verigene® is a gold nanoparticle-based formulation approved by FDA for diagnosis of Gram positive bacterial infections in blood stream [93]. This technology employs advanced automation for rapid detection of nucleic acids and proteins at the molecular level.

5.4 Challenges and Future Perspectives

Whether the nanoparticles for bio-imaging or therapy, the challenges are remaining same for clinical translation. Currently, nanoparticles are mostly used for healthcare applications because of their unique physicochemical properties. Especially, many researchers focused on development of various metal nanoparticle (AuNPs, AgNPs, SiNPs, iron NPs, etc.) based formulations for disease diagnosis and therapy. However, according to the experts, the toxicity concern of nanoparticles is not

completely addressed [94]. Further, investigation of nanoparticle interaction with the biomolecules (proteins, nucleic acids, lipids, and sugars) is very important to understand the toxicity profiles. Also, pharmacokinetics and pharmacodynamics are the crucial factors for evaluation of nanoparticle toxicity [95]. On the other hand, sometimes the in vitro toxicity responses of nanoparticles cannot be correlated with the in vivo systems without proper investigation. Therefore, toxicological investigation needs to be performed very carefully before translating them into human use. Additionally, bioavailability and clearance of nanoparticles is a major concern which should be undertaken for conducting the toxicity evaluation. Therefore, the functionalized nanoparticles should first pass through above stated criteria in order to keep them for the clinical use.

5.5 Conclusion

Several nanoparticles are emerged as probes for in vivo bio-imaging. Nanoparticles as imaging contrast agents are shown to be alternative for conventional small molecules for better imaging. Additionally, their less toxic effects and long circulation time enable them as the suitable candidates for bio-imaging. Moreover, multiphoton or upconversion based imaging methods make use of NIR light to acquire the images from deeper tissues. Despite of advantages, nanoparticle-based bio-imaging cannot completely replace the conventional imaging dyes or contrast agents due to some other issues like bio-degradability, immunogenicity, bio-availabilities, and clearance. Therefore, further research on nanotechnology is required for improving the effectiveness of the imaging techniques to diagnose the disease with more accuracy.

Acknowledgments The Authors are thankful to the Director, CSIR-IICT for his support and encouragement and for his keen interest in this work. IICT communication number IICT/Pubs./2019/113 dated March 25th 2019 for this manuscript is duly acknowledged.

References

1. Tempany CM, McNeil BJ. Advances in biomedical imaging. JAMA. 2001;285:562–7.
2. Sun Z, Ng KH, Ramli N. Biomedical imaging research: a fast-emerging area for interdisciplinary collaboration. Biomed Imag Interv J. 2011;7:e21.
3. Babic RR, Stankovic Babic G, et al. 120 years since the discovery of x-rays. Med Pregled. 2016;69:323–30.
4. Ding H, Wu F. Image guided biodistribution and pharmacokinetic studies of theranostics. Theranostics. 2012;2:1040–53.
5. Mettler FA Jr, Thomadsen BR, Bhargavan M, et al. Medical radiation exposure in the U.S. in 2006: preliminary results. Health Phys. 2008;95:502–7.
6. Power SP, Moloney F, Twomey M, et al. Computed tomography and patient risk: facts, perceptions and uncertainties. World J Radiol. 2016;8:902–15.
7. Larabell CA, Nugent KA. Imaging cellular architecture with X-rays. Curr Opin Struct Biol. 2010;20:623–31.

8. Grover VPB, Tognarelli JM, Crossey MME, et al. Magnetic resonance imaging: principles and techniques: lessons for clinicians. J Clin Exp Hepatol. 2015;5:246–55.
9. DiSanto RM, Subramanian V, Gu Z. Recent advances in nanotechnology for diabetes treatment. Wiley Interdiscip Rev Nanomed Nanobiotechnol. 2015;7:548–64.
10. Godin B, Sakamoto JH, Serda RE, et al. Emerging applications of nanomedicine for the diagnosis and treatment of cardiovascular diseases. Trends Pharmacol Sci. 2010;31:199–205.
11. Wang X, Yang L, Chen Z, Shin DM. Application of nanotechnology in cancer therapy and imaging. CA Cancer J Clin. 2008;58:97–110.
12. Yoon HY, Jeon S, You DG, et al. Inorganic nanoparticles for image-guided therapy. Bioconjug Chem. 2017;28:124–34.
13. Bigio IJ, Mourant JR. Ultraviolet and visible spectroscopies for tissue diagnostics: fluorescence spectroscopy and elastic-scattering spectroscopy. Phys Med Biol. 1997;42:803–14.
14. Kollias N, Zonios G, Stamatas GN. Fluorescence spectroscopy of skin. Vib Spectrosc. 2002;28:17–23.
15. Lai JP, Shah BP, Garfunkel E, Lee KB. Versatile fluorescence resonance energy transfer-based mesoporous silica nanoparticles for real-time monitoring of drug release. ACS Nano. 2013;7:2741–50.
16. Nakamura M, Hayashi K, Nakano M, et al. Identification of polyethylene glycol-resistant macrophages on stealth imaging in vitro using fluorescent organosilica nanoparticles. ACS Nano. 2015;9:1058–71.
17. Bhunia SK, Saha A, Maity AR, et al. Carbon nanoparticle-based fluorescent bioimaging probes. Sci Rep. 2013;3:1473.
18. Li Y, Zeng S, Hao J. Non-invasive optical guided tumor metastasis/vessel imaging by using lanthanide nanoprobe with enhanced down-shifting emission beyond 1500 nm. ACS Nano. 2019;13:248–59.
19. Kunjachan S, Ehling J, Storm G, et al. Noninvasive imaging of nanomedicines and nanotheranostics: principles, progress, and prospects. Chem Rev. 2015;115:10907–37.
20. Ntziachristos V. Going deeper than microscopy: the optical imaging frontier in biology. Nat Methods. 2010;7:603–14.
21. Hu S, Wang LV. Photoacoustic imaging and characterization of the microvasculature. J Biomed Opt. 2010;15:011101.
22. Kim C, Cho EC, Chen JY, et al. In vivo molecular photoacoustic tomography of melanomas targeted by bioconjugated gold nanocages. ACS Nano. 2010;4:4559–64.
23. Song KH, Kim CH, Cobley CM, et al. Near-infrared gold nanocages as a new class of tracers for photoacoustic sentinel lymph node mapping on a rat model. Nano Lett. 2009;9:183–8.
24. Chen YS, Frey W, Kim S, et al. Silica-coated gold nanorods as photoacoustic signal nanoamplifiers. Nano Lett. 2011;11:348–54.
25. Repenko T, Fokong S, De Laporte L, et al. Water-soluble dopamine-based polymers for photoacoustic imaging. Chem Commun. 2015;51:6084–7.
26. De La Zerda A, Zavaleta C, Keren S, et al. Carbon nanotubes as photoacoustic molecular imaging agents in living mice. Nat Nanotechnol. 2008;3:557–62.
27. Wu L, Cai X, Nelson K, et al. A green synthesis of carbon nanoparticles from honey and their use in real-time photoacoustic imaging. Nano Res. 2013;6:312–25.
28. Kircher MF, de la Zerda A, Jokerst JV, et al. A brain tumor molecular imaging strategy using a new triple-modality MRI-photoacoustic-Raman nanoparticle. Nat Med. 2012;18:829–34.
29. Beziere N, Lozano N, Nunes A, et al. Dynamic imaging of PEGylated indocyanine green (ICG) liposomes within the tumor microenvironment using multi-spectral optoacoustic tomography (MSOT). Biomaterials. 2015;37:415–24.
30. Ho CJH, Balasundaram G, Driessen W, et al. Multifunctional photosensitizer-based contrast agents for photoacoustic imaging. Sci Rep. 2014;4:5342.
31. Nie LM, Wang SJ, Wang XY, et al. In vivo volumetric photoacoustic molecular angiography and therapeutic monitoring with targeted plasmonic nanostars. Small. 2014;10:1585–93.
32. Kundu PP, Narayana C. Raman based imaging in biological application-a perspective. J Med Allied Sci. 2012;2:41.

33. Lu W, Singh AK, Khan SA, et al. Gold nano-popcorn-based targeted diagnosis, nanotherapy treatment, and in situ monitoring of photothermal therapy response of prostate cancer cells using surface-enhanced Raman spectroscopy. J Am Chem Soc. 2010;132:18103–14.
34. Moger J, Johnston BD, Tyler CR. Imaging metal oxide nanoparticles in biological structures with CARS microscopy. Opt Express. 2008;16:3408–19.
35. Lin L, Nufer K, Tomihara S, Prow T. Non-invasive nanoparticle imaging technologies for cosmetic and skin care products. Cosmetics. 2015;2:196–210.
36. Vanden-Hehir S, Tipping WJ, Lee M, et al. Raman imaging of nanocarriers for drug delivery. Nanomaterials (Basel). 2019;9:341.
37. Brown MA, Semelka RC, Dale BM. MRI: basic principles and applications. New York: Wiley; 2015.
38. Bulte JWM, Modo MMJ. Molecular and cellular MR imaging. Hoboken: CRC Press; 2007.
39. Bulte JWM, Kraitchman DL. Iron oxide MR contrast agents for molecular and cellular imaging. NMR Biomed. 2004;17:484–99.
40. Giovagnoni A, Fabbri A, Maccioni F. Oral contrast agents in MRI of the gastrointestinal tract. Abdom Imaging. 2002;27:367–75.
41. Penfield JG, Reilly RF. What nephrologists need to know about gadolinium. Nat Clin Pract Nephrol. 2007;3:654–68.
42. Kim BH, Lee N, Kim H, et al. Large-scale synthesis of uniform and extremely small-sized iron oxide nanoparticles for high-resolution T1 magnetic resonance imaging contrast agents. J Am Chem Soc. 2011;133:12624–31.
43. Lee N, Kim H, Choi SH, et al. Magnetosome-like ferrimagnetic iron oxide nanocubes for highly sensitive MRI of single cells and transplanted pancreatic islets. Proc Nat Acad Sci U S A. 2011;108:2662–7.
44. Lee N, Choi Y, Lee Y, et al. Water-dispersible ferrimagnetic iron oxide nanocubes with extremely high r2 relaxivity for highly sensitive in vivo mri of tumors. Nano Lett. 2012;12:3127–31.
45. Shin TH, Choi JS, Yun S, et al. T1 and T2 dual-mode MRI contrast agent for enhancing accuracy by engineered nanomaterials. ACS Nano. 2014;8:3393–401.
46. Ling D, Park W, Park SJ, et al. Multifunctional tumor pH-sensitive self-assembled nanoparticles for bimodal imaging and treatment of resistant heterogeneous tumors. J Am Chem Soc. 2014;136:5647–55.
47. Ma D, et al. NaGdF4:Yb3+/Er3+@NaGdF4:Nd3+@sodium-gluconate: multifunctional and biocompatible ultrasmall core–shell nanohybrids for UCL/MR/CT multimodal imaging. ACS Appl Mater Interfaces. 2015;7:16257–65.
48. Zhang XH, Blasiak B, Marenco AJ, et al. Design and regulation of NaHoF4 and NaDyF4 nanoparticles for high-field magnetic resonance imaging. Chem Mater. 2016;28:3060–72.
49. Lee N, Choi SH, Hyeon T. Nano-sized CT contrast agents. Adv Mater. 2013;25:2641–60.
50. Choudhury H, Cary R. Barium and barium compounds. Geneva: World Health Organization; 2001.. http://www.who.int/iris/handle/10665/42398
51. Galper MW, Saung MT, Fuster V, et al. Effect of computed tomography scanning parameters on gold nanoparticle and iodine contrast. Investig Radiol. 2012;47:475–81.
52. Stacul F, van der Molen AJ, Reimer P, et al. Contrast induced nephropathy: updated ESUR contrast media safety committee guidelines. Eur Radiol. 2011;21:2527–41.
53. Reuveni T, Motiei M, Romman Z, et al. Targeted gold nanoparticles enable molecular CT imaging of cancer: an in vivo study. Int J Nanomedicine. 2011;6:2859–64.
54. Bernstein AL, Dhanantwari A, Jurcova M, et al. Improved sensitivity of computed tomography towards iodine and gold nanoparticle contrast agents via iterative reconstruction methods. Sci Rep. 2016;6:26177.
55. Kim D, Park SJ, Lee JH, et al. Antibiofouling polymer-coated gold nanoparticles as a contrast agent for in vivo X-ray computed tomography imaging. J Am Chem Soc. 2007;129:7661–5.
56. Manohar N, Reynoso FJ, Diagaradjane P, et al. Quantitative imaging of gold nanoparticle distribution in a tumor-bearing mouse using benchtop x-ray fluorescence computed tomography. Sci Rep. 2016;6:22079.
57. Giepmans BNG, Adams SR, Ellisman MH, et al. Review - the fluorescent toolbox for assessing protein location and function. Science. 2006;312:217–24.

58. Kobayashi H, Ogawa M, Alford R, et al. New strategies for fluorescent probe design in medical diagnostic imaging. Chem Rev. 2010;110:2620–40.
59. Gamelin DR, Gudel HU. Design of luminescent inorganic materials: new photophysical processes studied by optical spectroscopy. Acc Chem Res. 2000;33:235–42.
60. Weissleder R. A clearer vision for in vivo imaging. Nat Biotechnol. 2001;19:316–7.
61. Larson DR, Zipfel WR, Williams RM, et al. Water-soluble quantum dots for multiphoton fluorescence imaging in vivo. Science. 2003;300:1434–6.
62. Yu JH, Kwon SH, Petrasek Z, et al. High-resolution three-photon biomedical imaging using doped ZnS nanocrystals. Nat Mater. 2013;12:359–66.
63. Cichy B, Wawrzynczyk D, Bednarkiewicz A, et al. Optical nonlinearities and two-photon excited time-resolved luminescence in colloidal quantum-confined CuInS2/ZnS heterostructures. RSC Adv. 2014;4:34065–72.
64. Subha R, Nalla V, Yu JH, et al. Efficient photoluminescence of Mn2+−doped ZnS quantum dots excited by two-photon absorption in near-infrared window II. J Phys Chem C. 2013;117:20905–11.
65. Betzig E, Patterson GH, Sougrat R, et al. Imaging intracellular fluorescent proteins at nanometer resolution. Science. 2006;313:1642–5.
66. Sochacki KA, Shtengel G, van Engelenburg SB, et al. Correlative super-resolution fluorescence and metal-replica transmission electron microscopy. Nat Methods. 2014;11:305–U278.
67. Zhu MQ, Zhang GF, Hu Z, et al. Reversible fluorescence switching of spiropyran-conjugated biodegradable nanoparticles for super-resolution fluorescence imaging. Macromolecules. 2014;47:1543–52.
68. Lin H, Choi Y, Lee Y, et al. Mapping of surface-enhanced fluorescence on metal nanoparticles using super-resolution photoactivation localization microscopy. Chem Phys Chem. 2012;13:973–81.
69. Auzel F. Upconversion and anti-stokes processes with f and d ions in solids. Chem Rev. 2004;104:139–73.
70. Lu YQ, Zhao JB, Zhang R, et al. Tunable lifetime multiplexing using luminescent nanocrystals. Nat Photonics. 2014;8:33–7.
71. Bunzli JCG, Piguet C. Taking advantage of luminescent lanthanide ions. Chem Soc Rev. 2005;34:1048–77.
72. Zhang F, Shi QH, Zhang YC, et al. Fluorescence upconversion microbarcodes for multiplexed biological detection: nucleic acid encoding. Adv Mater. 2011;23:3775–9.
73. Zheng XL, Zhu XJ, Lu YQ, et al. High-contrast visualization of upconversion luminescence in mice using time-gating approach. Anal Chem. 2016;88:3449–54.
74. Lee J, Yoo B, Lee H, et al. Ultra-wideband multi-dye-sensitized upconverting nanoparticles for information security application. Adv Mater. 2017;29:1603169.
75. Wu X, Zhang YW, Takle K, et al. Dye-sensitized core/active shell upconversion nanoparticles for optogenetics and bioimaging applications. ACS Nano. 2016;10:1060–6.
76. Wang F, Liu XG. Upconversion multicolor fine-tuning: visible to near-infrared emission from lanthanide-doped NaYF4 nanoparticles. J Am Chem Soc. 2008;130:5642.
77. Xie XJ, Gao NY, Deng RR, et al. Mechanistic investigation of photon upconversion in nd3+−sensitized core-shell nanoparticles. J Am Chem Soc. 2013;135:12608–11.
78. Park HS, Nam SH, Kim J, et al. Clear-cut observation of clearance of sustainable upconverting nanoparticles from lymphatic system of small living mice. Sci Rep. 2016;6:27407.
79. Jayakumar MKG, Bansal A, Li BN, et al. Mesoporous silica-coated upconversion nanocrystals for near infrared light-triggered control of gene expression in zebrafish. Nanomedicine. 2015;10:1051–61.
80. Yong-Dong K, Park TE, Singh B, et al. Image-guided nanoparticle-based siRNA delivery for cancer therapy. Curr Pharm Des. 2015;21:4637–56.
81. Iyer AK, He J, Amiji MM. Image-guided nanosystems for targeted delivery in cancer therapy. Curr Med Chem. 2012;19:3230–40.
82. Yu MK, Kim D, Lee IH, et al. Image-guided prostate cancer therapy using aptamer-functionalized thermally cross-linked superparamagnetic iron oxide nanoparticles. Small. 2011;7:2241–9.

83. Tomitaka A, Arami H, Raymond A, et al. Development of magneto-plasmonic nanoparticles for multimodal image-guided therapy to the brain. Nanoscale. 2017;9:764–73.
84. Satpathy M, Wang L, Zielinski RJ, et al. Targeted drug delivery and image-guided therapy of heterogeneous ovarian cancer using her2-targeted theranostic nanoparticles. Theranostics. 2019;9:778–95.
85. Le Duc G, Miladi I, Alric C, et al. Toward an image-guided microbeam radiation therapy using gadolinium-based nanoparticles. ACS Nano. 2011;5:9566–74.
86. Gao S, et al. Hybrid graphene/au activatable theranostic agent for multimodalities imaging guided enhanced photothermal therapy. Biomaterials. 2016;79:36–45.
87. Riley RS, Day ES. Gold nanoparticle-mediated photothermal therapy: applications and opportunities for multimodal cancer treatment. Wiley Interdiscip Rev Nanomed Nanobiotechnol. 2017;9:e1449.
88. Etame AB, Diaz RJ, O'Reilly MA, Smith CA, Mainprize TG, Hynynen K, Rutka JT. Enhanced delivery of gold nanoparticles with therapeutic potential into the brain using MRI-guided focused ultrasound. Nanomedicine. 2012;8:1133–42.
89. Mukherjee S, Chowdhury D, Kotcherlakota R, et al. Potential theranostics application of biosynthesized silver nanoparticles (4-in-1 system). Theranostics. 2014;4:316–35.
90. Patra CR, Mukherjee S, Kotcherlakota R. Biosynthesized silver nanoparticles: a step forward for cancer theranostics. Nanomedicine (Lond). 2014;9:1445–8.
91. Anselmo AC, Mitragotri S. Nanoparticles in the clinic. Bioeng Transl Med. 2016;1:10–29.
92. Thakor AS, Jokerst JV, Ghanouni P, et al. Clinically approved nanoparticle imaging agents. J Nucl Med. 2016;57:1833–7.
93. Scott LJ. Verigene® gram-positive blood culture nucleic acid test. Mol Diagn Ther. 2013;17:117–22.
94. Elsaesser A, Howard CV. Toxicology of nanoparticles. Adv Drug Deliv Rev. 2012;64:129–37.
95. Yildirimer L, Thanh NTK, Loizidou M, et al. Toxicology and clinical potential of nanoparticles. Nano Today. 2011;6:585–607.